Mon. Not. R. Astron. Soc. **000**, 1–7 (2004) Printed 5 February 2008 (MN LaTeX style file v2.2)

arXiv:astro-ph/0407031v1 1 Jul 2004

High Resolution Imaging of the HeII λ4686 Emission Line Nebula Associated with the Ultraluminous X-Ray Source in Holmberg II

P. Kaaret[1], M.J. Ward[2], A. Zezas[1]
[1] *Harvard-Smithsonian Center for Astrophysics, 60 Garden St., Cambridge, MA 02138, USA*
[2] *Department of Physics and Astronomy, University of Leicester, Leicester LE1 7RH, UK*

Accepted . Received ; in original form

ABSTRACT

We present Hubble Space Telescope images of the HeIII region surrounding the bright X-ray source in the dwarf irregular galaxy Holmberg II. Using *Chandra*, we find a position for the X-ray source of α = 08h 19m 28.98s, $\delta = +70^\circ 42' 19.''3$ (J2000) with an uncertainty of $0.6''$. We identify a bright, point-like optical counterpart centered in the nebula with the X-ray source. The optical magnitude and color of the counterpart are consistent with a star with spectral type between O4V and B3 Ib at a distance of 3.05 Mpc or reprocessed emission from an X-ray illuminated accretion disk. The nebular HeII luminosity is $2.7 \times 10^{36}\,\mathrm{erg\,s^{-1}}$. The morphology of the HeII, Hβ, and [OI] emission are consistent with being due to X-ray photoionization and are inconsistent with narrow beaming of the X-ray emission. A spectral model consisting of a multicolor disk blackbody with inverse-Compton emission from a hot corona gives a good fit to X-ray spectra obtained with XMM-Newton. Using the fitted X-ray spectrum, we calculate the relation between the HeII and X-ray luminosity and find that the HeII flux implies a lower bound on the X-ray luminosity in the range 4 to $6 \times 10^{39}\,\mathrm{erg\,s^{-1}}$ if the extrapolation of the X-ray spectrum between 54 eV and 300 eV is accurate. A compact object mass of at least 25 to $40 M_\odot$ would be required to avoid violating the Eddington limit.

Key words: black hole physics – galaxies: individual: Holmberg II – galaxies: starburst – galaxies: stellar content – X-rays: galaxies

1 INTRODUCTION

A key question in the study of the ultraluminous X-ray sources (ULXs) is whether or not the X-ray emission is beamed. If the X-rays are beamed, then the ULXs may be accreting "normal" mass ($< 20 M_\odot$) black holes or even neutron stars. King et al. (2001) have suggested that ULXs are high-mass X-ray binaries with super-Eddington mass transfer rates in which the X-ray emission is funnelled, producing high observed X-ray fluxes for observers near the beaming axis. Motivated by the recent suggestion that jets may contribute a significant fraction of the observed X-ray flux in Galactic binaries previously thought to be dominated by disk and coronal emission (Markoff, Falcke, & Fender 2001), Körding et al. (2002) have suggested that the ULXs may be stellar-mass black holes in which relativistic beaming in jets aligned nearly along our line of sight produce the high apparent X-ray fluxes.

If the ULXs are not strongly beamed, then the masses required for the sources to be emitting below their Eddington luminosities are large, well above the maximum possible mass ($\sim 20 M_\odot$) for a black hole produced at the endpoint of the evolution of a normal star. Hence, the compact objects would be "intermediate-mass" black holes (Colbert & Mushotzky 1999). This has potentially interesting consequences. Intermediate-mass black holes may be excellent sources of gravitational radiation (Ebisuzaki et al. 2001; Miller & Hamilton 2002). They may be relics of the first generation of star formation (Madau & Rees 2001), where, due to the absence of metals, extremely massive stars were likely to have formed (Larson 1998). Or, they may be important in the formation of supermassive black holes (Ptak & Griffiths 1999).

Pakull & Mironi (2002) discovered an HeII λ4686 emission line nebula in the ROSAT error box for the ULX in the dwarf irregular galaxy Holmberg II at a distance of 3.05 Mpc (Hoessel, Saha, & Danielson 1998). X-ray emission was first detected from Holmberg II in the ROSAT all-sky survey and then localized in ROSAT

© 2004 RAS

HRI observations to a single, highly variable source with a maximum luminosity (if isotropic) of $\sim 10^{40}\,\mathrm{erg\,s^{-1}}$ (Zezas, Georgantopoulos, & Ward 1999). If a ULX is embedded in a diffuse nebula, then the X-radiation of the ULX should photoionize the nebula, as seen for the nebula surrounding LMC X-1 (Pakull & Angebault 1986). Photoionization produces (at most) one optical/UV photon for each X-ray photon doing the excitation, so the line flux from the nebula is a direct measure of the total number of ionizing photons emitted in all directions. For example, measurement of the HeII λ4686 flux gives a direct count of all source photons with energies above 54 eV which ionize the nebula. The discovery of an HeIII region near a ULX offers the exciting prospect of determining observationally whether or not the X-ray emission from the ULX is beamed. If the ULX is truly ultraluminous, then the X-ray photoionization should produce observable UV and optical line emission from high excitation levels. Pakull & Mironi (2002) report an inferred photoionization luminosity of $(3-13)\times10^{39}\,\mathrm{erg\,s^{-1}}$ for a distance of 3.2 Mpc based on an assumed thermal bremsstrahlung X-ray spectrum, X-ray spectral measurements from the ROSAT PSPC (Fourniol 1998) and ASCA (Miyaji, Lehman, and Hasinger 2001), and modelling of the photoionization nebula. The lower end of their allowed luminosity range is consistent with the highest luminosities observed from stellar-mass black hole candidate X-ray binaries within the Milky Way.

Here, we report on Hubble Space Telescope observations of the vicinity of the ULX in Holmberg II taken in the optical emission lines HeII λ4686, Hβ, and [OI] λ6300, new Chandra High-Resolution Camera observations, and archival XMM-Newton data. The improved X-ray position from Chandra strengthens the association of the nebula with the X-ray source. The HST images enable detailed inspection of the morphology of the nebula and allow us to isolate it from other nearby nebulosities. The XMM-Newton data provide high quality information on the X-ray spectrum which are essential to constraining the true luminosity of the system. We describe the observations and analysis in § 2, and discuss the implications in § 3.

2 OBSERVATIONS AND ANALYSIS

2.1 Chandra Observations

Observations of Holmberg II were made using the High-Resolution Camera (HRC) onboard the Chandra X-Ray Observatory (ObsID 3816; PI Kaaret). The HRC was used and the source was placed off-axis to prevent pile-up from affecting the position determination. The *Chandra* observation began on 3 July 2003 05:56:20 UT and had a useful exposure of 4.9 ks. Chandra data were subjected to standard processing and event screening. No strong background flares were found, so the entire observation was used. A bright source is detected at high significance which we identify with the ULX in Holmberg II (Zezas, Georgantopoulos, & Ward 1999; Kerp, Walter, and Brinks 2002). The *Chandra* position is: α = 08h 19m 28.98s, $\delta = +70^\circ42'19.''3$ (J2000). This position is determined using the *Chandra* aspect solution, which has an estimated uncertainty of $0.6''$ at 90% confidence (see the Chandra aspect pages at http://cxc.harvard.edu/cal/ASPECT/celmon). The X-ray image is consistent with that expected for a point source at the given position off-axis. We find no evidence for a significant extended component as reported by Miyaji et al. (2001).

2.2 XMM-Newton data

We extracted observations of Holmberg II from the XMM-Newton archive. Analysis of these data have been previously reported by Dewangan et al. (2004). We reduced the data and generated response matrices using the SAS software version 5.4.1. We use only data from the EPIC-PN. We examined the three useful available observations. The first observation occurred on 10 April 2002 (ID 0112520601; PI Watson). The time on-target was 5.1 ks, during which the total PN rate was always below 20 c/s indicating there were no background flares. The total exposure after live time correction was 4.7 ks. The second observation occurred on 16 April 2002 (ID 0112520701; PI Watson). There were several background flares, so we filtered the data to remove times with PN count rates above 35 c/s. The third observation occurred on 19 Sept 2002 (ID 0112520901; PI Watson). There were, again, background flares and we filtered the data to removed times with PN count rates above 20 c/s. Spectra were extracted from circular regions with a radius of $24''$. For all observations, the source was located near a chip edge, and we used circular background regions on the same chip. The spectra were regrouped to have at least 100 counts per bin for the first two observations and 25 counts per bin for the last. Models were fitted to the spectra using XSPEC version 11.2 over an energy band from 0.3 to 8 keV.

As found by Dewangan et al. (2004), complex or multicomponent models are required to obtain adequate fits. A model consisting of the sum of powerlaw plus disk blackbody emission each modified by interstellar absorption has often been used to model the spectra of black hole X-ray binaries and ultraluminous X-ray sources. Using such a model, we find best-fitting parameters similar to those reported by Dewangan et al. (2004).

A key input to the photoionization modelling is the X-ray spectrum. To input to the photoionization code, we must extrapolate the fitted X-ray spectrum to energies below the minimum observed X-ray energy; the shape of the spectrum between 54 eV and 300 eV is important in determining the relation between the HeII luminosity and the X-ray luminosity. In the powerlaw plus disk blackbody model, the powerlaw component is an adhoc model for a Compton emission component arising from disk photons inverse-Compton scattered by energetic electrons in a corona. This suggests that the powerlaw component should be cut off at energies below the disk temperature. However, the model contains no prescription for the form of such a cutoff. We require a model in which the low energy extension of the spectrum is well defined and physically motivated. Based on the application of Comptonization models for detailed physical modelling of the multiwavelength spectral of black hole X-ray binaries, we choose to use a Comptonization model (Poutanen & Svensson 1996). Specifically, we use the model of Poutanen & Svensson (1996), *compps* in XSPEC, to calculate the spectrum produced by thermal Comptonization of photons emitted with a disk blackbody spectrum and scat-

Observation	$kT_{\rm in}$ [keV]	kT_e [keV]	τ	$L_{\rm X}$ [erg cm^{-2} s^{-1}]	$L_{\rm PI}$ [erg s^{-1}]
10 April	$0.22^{+0.02}_{-0.08}$	49 ± 14	$1.1^{+0.3}_{-0.4}$	16×10^{39}	5.9×10^{39}
16 April	0.20 ± 0.02	76 ± 23	0.8 ± 0.3	17×10^{39}	6.1×10^{39}
19 Sept	0.17 ± 0.02	71 ± 30	$0.4^{+0.4}_{-0.2}$	5×10^{39}	3.7×10^{39}

Table 1. X-Ray Spectral Fits. Best fit spectral parameters for each observation. The table includes: the date in 2002 of the observation; the temperature of the multicolor disk blackbody emission, $kT_{\rm in}$; the temperature, kT_e, and optical depth, τ, of the hot electron corona; the total intrinsic X-ray luminosity inferred from the X-ray flux and the Comptonization model parameters assuming isotropic emission, $L_{\rm X}$; and the total photoionization luminosity, $L_{\rm PI}$, required to produce the observed HeII luminosity using the fitted X-ray spectrum as input to *Cloudy*. The errors correspond to 90% confidence for a single parameter ($\delta chi^2 = 2.71$).

tered in a hot corona. The model parameters allowed to vary in the fits are the disk temperature $kT_{\rm in}$, the corona electron temperature kT_e, and the corona optical depth τ.

Because the metallicity of Holmberg II is significantly lower than solar, we use two absorption components: one to model absorption within the Milky Way for which we fix the metallicity at solar and fix the absorption column density $N_{\rm H} = (3.42 \pm 0.3) \times 10^{20}\,{\rm cm}^{-2}$, and a second to model absorption within Holmberg II for which we fix the metallicity at $Z = 0.07 Z_{\odot}$ (Mirioni 2002). We performed a simultaneous fit to the data for all three observations in which the absorption within Holmberg II was the same for all observations and the Comptonization model parameters were allowed to vary individually for each observation. We found an adequate fit with $\chi^2/{\rm DoF} = 273.5/285$. The best fit parameters are reported in Table 1. The best fit column density is $(3.7 \pm 0.5) \times 10^{21}\,{\rm cm}^{-2}$. We note that this column density is significantly above that found by Dewangan et al. (2004) because the absorption, beyond the Galactic component, is calculated for the low metallicity appropriate to Holmberg II.

The three XMM-Newton observations cover the extremes of X-ray flux detected from Holmberg II X-1 (Dewangan et al. 2004). Therefore, these observations also likely cover the range of X-ray spectral variations in the source.

We note a thermal bremsstrahlung model as used by Pakull & Mirioni (2002) for input to their photoionization modelling does not provide an adequate fit to any of the observations, even with use of two distinct absorption components.

2.3 HST observations

Observations were made of Holmberg II centered on the position of the ULX using the Advanced Camera for Surveys (ACS) on the Hubble Space Telescope (HST) under GO program 9684 (PI Kaaret). Observations were made in the narrow band filters FR462N centered on HeII λ4686, FR505N centered on Hβ λ4861, and FR656N centered on [OI] λ6300. Images in the FR462N filter were obtained on 21 January 2003 and 25 June 2003. For the January observation, the aimpoint was placed closed to the ramp filter edge and there are non-uniformities in transmission across the image. For this reason, we quote fluxes for the HeII emission based only on the June observation. The images in all of the other filters were obtained on 24 November 2002. All of the narrow band filters have a 2% bandwidth. The recession velocity of Holmberg II is 157 km/s (Strauss et al. 1992), so the redshifted emission lines lie within the filter bandpasses. In addition, observations were made in the medium filters FR459M and F550M for continuum imaging and continuum subtraction.

The standard processing for ACS data does not perform cosmic-ray removal for images without cosmic-ray splits. Because all of our observations except those in the FR462N filter were performed in dither patterns without cosmic-ray splits, we re-processed all observations using the *PyRAF* task *multidrizzle* in STSDAS 3.1 to remove the cosmic ray hits. We found residual sky level offsets in the images and removed these by fitting a gaussian to those pixels not containing astronomical objects in a $30'' \times 30''$ field centered near the ULX and subtracting off the gaussian centroid. We aligned the F550M (narrow V band) image to 10 stars selected from the USNO A2.0 catalog (Monet et al. 1996) using the *imwcs* tool from the Smithsonian Astrophysical Observatory Telescope Data Center. Based on the residual offsets for the 10 stars, we estimate that the astrometric uncertainty is $0.3''$. We then aligned each other image to the aspect corrected F550M image using the *IRAF* tools *geomap* and *geotran* (Tody et al. 1993). We checked the alignment using the tool *xregister* and found that the residual misalignments were less than 0.1 pixel.

We produced continuum subtracted images using the FR459M image to estimate the continuum for the FR462N HeII λ4686 and FR505N Hβ λ4861 images, and the F550M image to estimate the continuum for the FR656N [OI] λ6300 image. Since we are interested primarily in the diffuse, nebular emission, we located the stars in each frame and subtracted off the stellar emission before performing the continuum subtraction. We fit a Moffat profile to several bright stars to determine the point spread function shape, and then used that fixed shape in fitting and subtracting the stars. We note that the FR459M image used for continuum subtraction of the FR462N image contains the HeII line. We correct for the apparent reduction in the HeII line flux caused by partial subtraction of the line as described below.

For the continuum subtraction of the nebula, we assumed that the intrinsic continuum spectrum is flat, $F(\lambda) \propto \lambda^n$ with $n = 0$ and reddened with an extinction of E(B-V) = 0.024 (Stewart et al. 2000). For the HeII and Hβ images, the continuum band lies close to the line wavelength, and changing the continuum slope does not significantly affect the estimated line flux (we discuss this further below in the estimation of the total HeII line flux). For [OI], the line wavelength lies further from the best continuum band available. For [OI], we repeated this procedure using continuum slopes

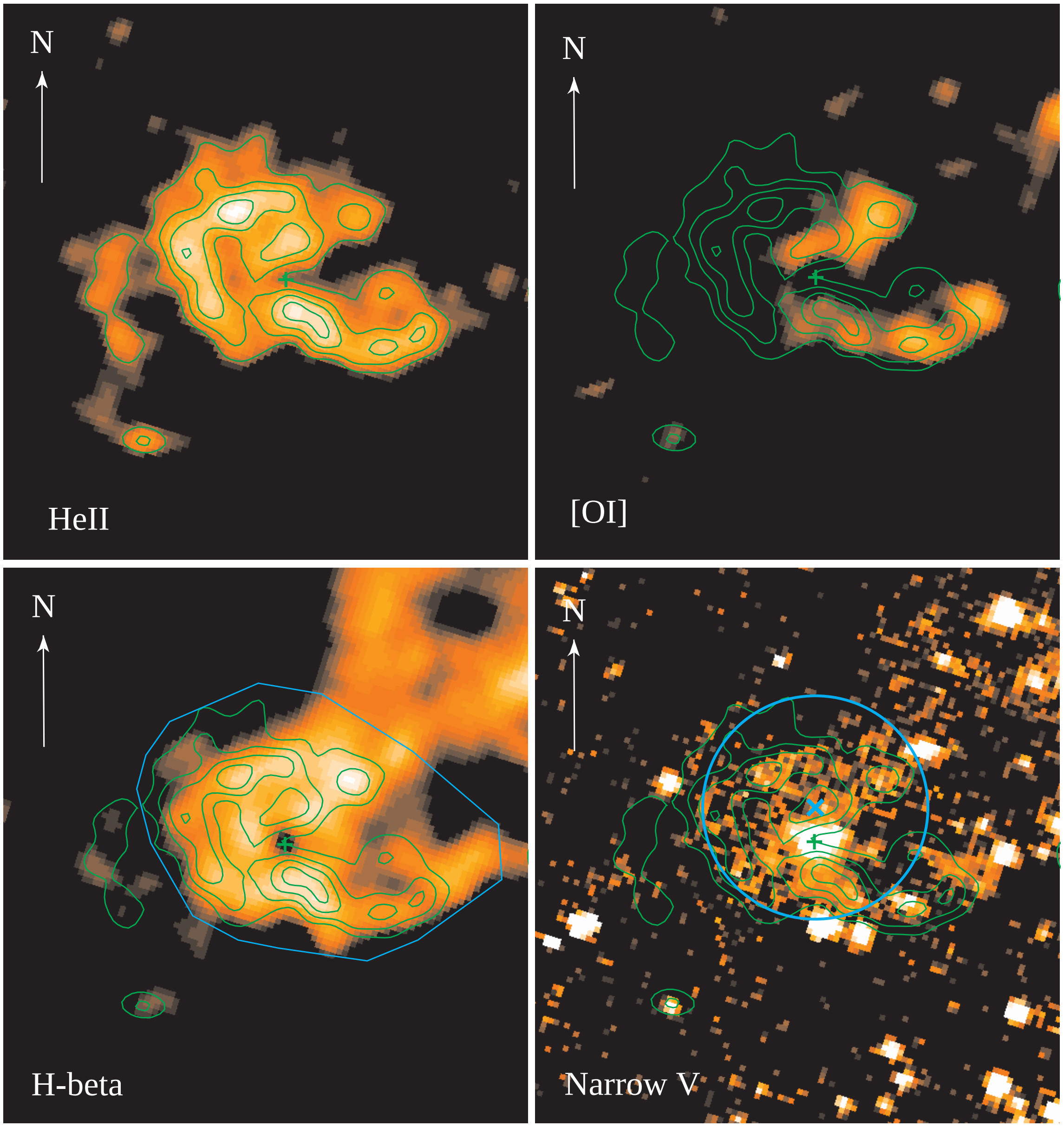

Figure 1. False color images of the continuum subtracted line emission for He II λ4686, Hβ λ4861, and [O I] λ6300 and for the narrow V-band continuum. In each image, the arrow points Northward and has a length of 1″ (15 pc), East is to the left, the green cross marks the position of the bright star within the nebula, and the green curves are contours of the He II emission. The contour levels are $[2, 3, 4, 5] \times 1.9 \times 10^{-16}$ erg cm^{-2} s^{-1} arcsec^{-2}. The same contours are plotted on all four panels. The cyan circle and 'X' in the narrow-V image denote the best Chandra position for the ULX and the relative Chandra/HST error circle. The cyan polygon in the Hβ image shows the region used for the line flux measurements described in the text. Each line image was smoothed with a gaussian filter with a FWHM of 0.24″.

$n = +2$ and $n = -2$. We found that the morphology of the [O I] emission varied little. Fig. 1 shows the continuum subtracted images in the three lines and the F550M (narrow V band) continuum image. The He II nebula reported by Pakull and Mironi (2002) is clearly detected and is at a position consistent with that of the X-ray source.

There is one bright point source within the nebula visible in the narrow V-band image. The source profile appears similar to those of other stars in each image and there is no evidence for spatial extent. The source appears to be a star, but a compact core of the nebula, unresolved at the resolution of the ACS/WFC, could also contribute to the emission. The position of the star is α = 08h 19m 28s.99 and $\delta = +70^\circ\ 42'\ 19''.0$ (J2000). This is 0.3″ from the Chandra position for the X-ray source. This offset is less than the relative astrometric uncertainty between the Chandra and HST images. Therefore, we consider the optical star to be the counterpart of the X-ray source. We find the ST magnitudes of the star to be 22.04 ± 0.08 in the F550M filter and 21.35 ± 0.10 in the FR459M filter. The dominant uncertainty is in the removal of the underlying nebular component. If we consider only the extinction within the Milky Way, then the reddening-corrected equivalent Johnson V magnitude is 21.86 ± 0.09 and the color $(\mathrm{B}-\mathrm{V})_0 = -0.20 \pm 0.15$. Conversion to standard Johnson magnitudes increases the quoted uncertainty because the filters used only approximately match the Johnson bands. There may also be extinction within Holmberg II. Using the relation between N_H and $E(B-V)$ determined for the SMC (Bouchet et al. 1985), we find $E(B-V) = 0.07 \pm 0.01$ based on our spectral fit to XMM-Newton data. This is an upper bound on the reddening since it is not clear whether the column density observed towards the X-ray source necessarily obscures the companion star. In some Galactic black holes, the X-ray absorption is seen to vary on a time scale of minutes, indicating that the absorption occurs close to the compact object (Tomsick, Lapshov, Kaaret 1998). Applying this additional reddening with an SMC extinction law, we find a Johnson V magnitude of 21.64 ± 0.11 and a color $(\mathrm{B}-\mathrm{V})_0 = -0.25 \pm 0.16$.

To estimate the HeII λ4686 line flux from the nebula, we found the total count rates for the nebula in the FR462N and FR459M images from which the stellar emission had been subtracted. We defined the nebula using a contour drawn to enclose the HeII and Hβ emission which is shown as a cyan curve in the Hβ image in Fig. 1. The FR459M filter bandpass included the HeII λ4686 emission line (unfortunately, the FR459M bandpass is too wide to exclude both HeII and the stronger Hβ and Hγ emission from the nebula). Hence, we must solve for the HeII line flux and the continuum flux given the nebular count rates in the two filters. We assumed that the nebular continuum emission has a power-law spectrum $F(\lambda) \propto \lambda^n$. We used the *IRAF* tool *calcphot* in the *synphot* package with HST/ACS calibration files released on 10 Dec 2003 to find count rates in each filter for given continuum flux and HeII line flux. We then inverted the matrix relating the fluxes to count rates and calculated the fluxes from the measured count rates. For a flat continuum with $n = 0$, we find that the flux in the HeII line is $2.4 \times 10^{-15}\,\mathrm{erg\,cm^{-2}\,s^{-1}}$. Our continuum subtraction procedure depends on the assumed continuum shape. Repeating the procedure for $n = +2$ and $n = -2$, we find that the uncertainty in the HeII line flux induced by the uncertainty in the continuum slope is of order 3%. Including additional factors such as the uncertainties in the subtraction of the stars, the calibrations of the filters, and the subtraction of the sky background, we estimate an overall uncertainty in our HeII flux measurement of 9%.

Using the same contour defined for the HeII, which was drawn to enclose both the HeII and Hβ emission, we found the flux in Hβ of $1.1 \times 10^{-14}\,\mathrm{erg\,cm^{-2}\,s^{-1}}$ and in [OI] of $1.3 \times 10^{-15}\,\mathrm{erg\,cm^{-2}\,s^{-1}}$. The uncertainty on the Hβ flux is 5% and on the [OI] is 20%. We find a ratio HeII/Hβ = 0.22 ± 0.02. This is larger than the value of 0.16 found by Pakull and Mironi (2002), but the difference may be due to sampling of a larger spatial region due to the effect of seeing in their ground-based spectrum. To test this, we convolved our image with a gaussian with 2.0″ FWHM and then extracted fluxes from a circular region with the same area as the contour defined in Fig. 1. We find HeII/Hβ = 0.18±0.02, consistent with Pakull and Mironi (2002). The ratio is at the extreme end of the range found in photoionized nebulae in nearby galaxies (Garnett et al. 1991).

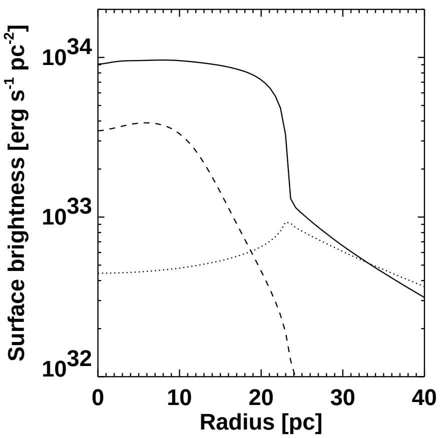

Figure 2. Surface brightness of optical lines in a simulation of a photoionized nebula produced with *Cloudy* with a nebular hydrogen density of 10 cm^{-3}. The solid line is for Hβ λ4861, the dashed line for HeII λ4686, and the dotted line for [OI] λ6300. The surface brightness was calculated by integrating the emissivity predicted by *Cloudy* for a spherical nebula with uniform density along lines of sight through the nebula. The actual nebula is not spherically symmetric and may have varying density.

3 INTERPRETATION

We confirm the discovery by Pakull and Mironi (2002) of a HeII λ4686 emission line nebula near the ultraluminous source in Holmberg II. Our improved X-ray astrometry derived from *Chandra* strengthens the association of the nebula with the X-ray source.

We detect one point-like source within the body of the nebula. This source is likely the optical counterpart to the ULX. For a distance to Holmberg II of 3.05 Mpc, the absolute magnitude M_V of this source is between -5.5 and -5.9 depending on whether there is reddening within Holmberg II as discussed in section 2.3. The absolute magnitude and B-V color are consistent a range of spectral types from O4V to B3 Ib. We note that this spectral classification is valid only if there is no significant contribution of optical light from the accretion disk and if the star is not significantly affected by the gravitational pull or X-ray emission from the compact object. Alternatively, the optical emission may be reprocessed emission from an X-ray illuminated accretion disk. The ratio of observed X-ray to optical flux and the B-V color are consistent with those found for low-mass X-ray binaries in which the optical emission is dominated by an X-ray illuminated disk (van Paradijs & McClintock 1995).

Other optical counterpart searches have found early-type stellar counterparts to ultraluminous X-ray sources. The optical counterpart to M81 X-6 (Fabbiano 1988) has colors consistent with an O8V star, although there is some uncertainty in the spectral type due to significant reddening (Liu, Bregman, & Seitzer 2002). For NGC 1313 X-2, only the R magnitude of the counterpart has been measured; the absolute magnitude is consistent with an early O main sequence star or an OB supergiant (Zampieri et al. 2004). In NGC 5204, the optical counterpart found on ground-based images (Roberts et al. 2001) was resolved into two sources with HST images (Goad et al. 2002).

For Holmberg II, Pakull and Mironi (2002) report that the HeII λ4686 emission has a FWHM of 2.2″ and that the [OI] is offset to the West of the HeII emission. Our HST images confirm these basic results and provide much more detailed information on the morphology of the nebula.

The maximum extent of the HeII emission is to the West of the central star and is about 1.7″ or 26 pc for a distance to Holmberg II of 3.05 Mpc. The extent of the nebula towards the East is shorter, about 1.0″ or 15 pc. To the West of the central star (from NW to SW), the morphology of the Hβ emission is similar to, but more extended than, that of the HeII emission and [OI] emission is low close to the star and stronger farther out, particularly past the point where the HeII emission peaks. This is consistent with the behaviour expected for a photo-ionized nebula. HeII emission is produced in regions of high excitation and should be concentrated near the central source. Hβ is produced over a broad range of excitation and should cover a larger spatial range than HeII. [OI] is preferentially produced at lower excitation than HeII and should be produced in the outer regions of the nebula. Hence, the relative morphologies of the HeII, Hβ, and [OI] emission support the hypothesis that the nebula is photoionized (Pakull & Mirioni 2002). Fig. 2 shows the surface brightness versus radius calculated for a photoionized nebula (discussed further below) for comparison.

To the East and South of the central star, the morphology of the Hβ emission is very similar to that of the HeII emission and [OI] emission is absent. This is also consistent with a X-ray photoionized nebula if the column density of the nebula integrated along line of sight outward from the central star, is sufficiently small that the entire nebula to the East and South is excited to produce HeII emission (Pakull & Mirioni 2002).

We note that there is additional Hβ emission to the NW of the central star and beyond the extent of the HeII emission which appears to be part of a ring nebula surrounding a bright star visible in the narrow V band image and unrelated to the HeII nebula. Also, the isolated HeII bright spot to the SE of the central star appears to be due to incomplete subtraction of a star visible in the narrow V band image.

If the nebula is powered by X-ray photoionization from the central source, then the morphology of the nebula appears inconsistent with narrow beaming of the X-ray emission.

The HeII nebular emission is likely isotropic. Therefore, the measured flux should provide a good estimate of the true luminosity. For a distance to Holmberg II of 3.05 Mpc, the HeII λ4686 line flux found here for the nebula implies a line luminosity of 2.7×10^{36} erg s^{-1}. This is consistent with the value reported by Pakull & Mironi (2002).

HeII λ4686 emission is produced via the recombination of doubly ionized He^{++} and acts as a photon counter of radiation ionizing the nebula in the He^{+} Lyman continuum above 54 eV. Following Pakull & Mironi (2002), we use this property to estimate the true luminosity of the X-ray source. The major uncertainty in their estimate was imprecise knowledge of the shape of the photon spectrum illuminating the nebula. Using the XMM-Newton spectra, we are able to reduce this uncertainty.

We used the photoionization code *Cloudy* version 94.00 (Ferland 2001) to estimate the true X-ray luminosity based on the measured HeII luminosity. We used a metallicity of $Z = 0.07 Z_{\odot}$ (Mirioni 2002). The relation between the total HeII flux and the total ionizing X-ray flux is not sensitive to the metallicity. We ran simulations over a range of hydrogen density within the nebula from 1 to 100 cm^{-3}. The relation between the total HeII flux and the total ionizing X-ray flux is not sensitive to the density as long as the region of fully ionized He is contained within the simulated nebula. The spatial extent of the HeII emitting region is sensitive to the density. A constant density of 10 cm^{-3} gave a reasonable match to the observed spatial extent of the HeII emission, and we use this value in the simulations presented here. In the modeling, we assumed a spherical geometry with a filling factor of unity. We assumed that there is no absorption between the X-ray source and the nebula. We also include the photon flux of an O5V star modelled as a blackbody with a temperature 42000 K and a luminosity of 3.2×10^{39} erg s^{-1}. Fig. 2 shows the calculated surface brightness versus apparent offset from the X-ray source. The surface brightness was calculated by integrating the emissivity along lines of sight through a spherically symmetric nebula.

Table 1 shows the photoionization luminosities required to produce the measured HeII luminosity for the various best fit Comptonization spectra. The inferred photoionization luminosities range from 3.7 to 6.1×10^{39} erg s^{-1}. The low luminosity value comes from the September 2002 observation during which the source was in an unusual low/soft state (Dewangan et al. 2004). The correct X-ray spectrum to use in the photoionization modelling would be a luminosity weighted average of observed spectra sampling a duration comparable to the recombination time of He^{++} in the nebula, roughly 3000 years for an electron density of 10 cm^{-3} and temperature of 20,000 K. The luminosity weighting would suggest a photoionization luminosity near the high end of the range.

To test the sensitivity of these results to the flux from the companion star, we also made runs with the O5V star replaced by a B2 Ib star modelled as a blackbody with a temperature 18,500 K and a luminosity of 2×10^{38} erg s^{-1}. The inferred photoionization luminosities increase by 12 to 16% if a B2 Ib star is used in place of the O5V star.

As noted above, our photoionization model assumes a covering factor of unity and sufficient depth radially so that the entire X-ray flux of the central source is absorbed. Inspection of the HeII line emission image shows that the covering factor is below unity. Also, as described above, [OI] emission should be present at larger radii than the HeII emission if the nebula is not density bounded. Comparison of the [OI] and HeII images shows the nebula is density bounded to the East and South of the central star. Therefore, the photoionization luminosity quoted here should be considered a lower bound to the total luminosity of the ionizing radiation. Partial absorption intrinsic to the X-ray source would harden the soft X-ray flux illuminating the nebula and would increase the required luminosity. The unabsorbed X-ray luminosity in the Comptonization models, assuming isotropic emission, ranges from 5 to 17×10^{39} erg s^{-1} for the three observations. This is consistent with the luminosity inferred from the HeII emission, given that the HeII emission likely underestimates the true luminosity due to the covering factor of the nebula being less than one and the nebula being density bounded along several lines of sight.

We conclude that the X-ray and HeII data are consistent with the X-ray source being the ionization source powering the line emission from the nebula. The luminosity in HeII emission is more than an order of magnitude greater than that observed from a similar nebula around the black hole candidate LMC X-1 (Pakull & Angebault 1986), suggesting that Holmberg II contains a much more powerful X-ray source. We estimate that the total luminosity of the X-ray source is at least $3.3 \times 10^{39}\,\mathrm{erg\,s^{-1}}$ and likely above $6 \times 10^{39}\,\mathrm{erg\,s^{-1}}$ if the extrapolation of the X-ray spectrum between 54 eV and 300 eV is accurate. This suggests that the compact object is truly ultraluminous. Assuming an Eddington luminosity of $1.3\times10^{38}\,\mathrm{erg\,s^{-1}M_{\odot}^{-1}}$, the compact object mass would be at least $25M_{\odot}$ and likely above $40M_{\odot}$. This may suggest a compact object which is more massive than the stellar-mass black holes candidates in our Galaxy, for which all of the dynamically measured masses lie below $20M_{\odot}$ (McClintock & Remillard(2003)).

ACKNOWLEDGMENTS

We thank the Aspen Center for Physics for its hospitality during the workshop "Compact Objects in External Galaxies" and an anonymous referee for comments which improved this manuscript. PK thanks Manfred Pakull for useful discussions and Manfred Pakull and Laurent Mirioni for a copy of Laurent Mirioni's thesis. PK acknowledges partial support from STScI grant HST-GO-09684.01 and Chandra grant CXC GO3-4052X. AZ acknowledges partial support from NASA LTSA grant NAG5-13056. STSDAS and PyRAF are products of the Space Telescope Science Institute, which is operated by AURA for NASA.

REFERENCES

Bouchet P., Lequeux J., Maurice E., Prévot L., Prévot-Burnichon M.L. 1985, A&A, 149, 330
Colbert, E.J.M. & Mushotzky, R.F. 1999, ApJ, 519, 89
Dewangan G.C., Miyaji T., Griffiths R.E., Lehmann I. 2004, ApJ, submitted, astro-ph/0401223
Ebisuzaki T. et al. 2001, ApJ, 562, L19
Fabbiano G. 1988, 325, 544
Ferland G.J. 2001, Hazy, a brief introduction to Cloudy 96.00
Fourniol N. 1998, Thesis, Université de Strasbourg
Garnett D.R., Kennicutt R.C., Chu Y.-H., Skillman E.D. 1991, PASP, 103, 850
Goad M.R., Roberts T.P., Knigge C., Lira P. 2002, MNRAS, 335, L67
Hoessel J.G, Saha A., & Danielson G.E. 1998, AJ, 115, 573
Kerp J., Walter F., Brinks E. 2002, ApJ, 571, 809
King A.R., Davies M.B., Ward M.J., Fabbiano G., Elvis M. 2001, ApJ, 552, L109
Körding E., Falcke H., Markoff S. 2002, A&A, 382, L13
Larson R.B. 1998, MNRAS, 301, 569
Liu J.-F., Bregman J.N., Seitzer P. 2002, ApJ, 580, L31
Liu J.-F., Bregman J.N. 2003, American Astronomical Society Meeting 203, #81.09
Madau P. & Rees R.J. 2001, ApJ, 551, L27
Makishima K. et al. 2000, ApJ, 535, 632
Markoff S., Falcke H., Fender R. 2001, A&A, 372, L25
McClintock J.E. & Remillard R.A. 2003, astro-ph/0306213
Miller, M.C. & Hamilton, D.P. 2002, MNRAS, 330, 232
Mirioni L. 2002, Thesis, University of Strasbourg
Miyaji T., Lehman I., Hasinger G. 2001, ApJ, 121, 3047
Monet, D. et al. 1996, USNO-SA1.0, (U.S. Naval Observatory, Washington DC).
Pakull M.W., Angebault L.P. 1986, Nature, 322, 511
Pakull M.W., Mirioni L. 2002, astro-ph/0202488
Poutanen J., Svensson R. 1996, ApJ, 470, 249
Ptak A., Griffiths R. 1999, ApJ, 517, L85
Roberts T.P., Goad M.R., Ward M.J., Warwick R.S., O'Brien P.T., Lira P., Hands A.D.P. 2001, MNRAS, 325, L7
Stewart S.G. et al. 2000, ApJ, 529, 201
Strauss M.A., Huchra J.P, Davis M., Yahil A., Fisher K.B., Tonry J. 1992, ApJS, 83, 29
Tody E. 1993, in Astronomical Data Analysis Software and Systems II, A.S.P. Conference Ser., Vol. 52, eds. R.J. Hanisch, R.J.V. Brissenden, & J. Barnes, 173.
Tomsick J.A., Lapshov I., Kaaret P. 1998, ApJ, 494, 747
van Paradijs J., McClintock J.E. in X-Ray Binaries, eds. W.H.G. Lewin, J. van Paradijs, & E.P.J. van den Heuvel, (Cambridge Univ. Press, 1995), pp. 58-125.
Zampieri L., Mucciarelli P., Falomo R., Kaaret P., Di Stefano R., Turolla R., Chieregato M., Treves A. 2004, ApJ, in press, astro-ph/0310739
Zezas A.L., Georgantopoulos I., Ward M.J. 1999, MNRAS, 308, 302